Advanced Piezo-Active 2–1–2 Composites with Large Parameters for Hydroacoustic and Energy-Harvesting Applications

V. Yu. Topolov(✉)

Department of Physics, Southern Federal University, 5 Zorge Street, 344090 Rostov-on-Don, Russia
vutopolov@sfedu.ru

Abstract. Novel piezo-active 2–1–2 composites with two single-crystal components are studied to show their large hydrostatic parameters and figures of merit concerned with the hydrostatic, longitudinal, and transverse piezoelectric effects. The 2–1–2 composite contains layers of domain-engineered [0 1 1]-poled relaxor-ferroelectric $(1 - x)Pb(Zn_{1/3}Nb_{2/3})O_3 - xPbTiO_3$ single crystal ($x = 0.0475$–0.09) and layers that contain aligned piezoelectric $Li_2B_4O_7$ single crystal rods in polyethylene, and these layers are distributed regularly and in the form of an elliptic cylinder. Due to the microgeometry of the composite and the piezoelectric properties of the single-crystal components, large values of the hydrostatic figure of merit $d_h^* g_h^* > 2 \cdot 10^{-10}$ Pa^{-1} and longitudinal figure of merit $d_{33}^* g_{33}^* \sim 10^{-10}$ Pa^{-1} are achieved in specific volume-fraction and aspect-ratio range, at relatively small volume fractions of the single-crystal rods. An effect of the aspect ratio of the rod base on the piezoelectric performance and figures of merit if the composite is discussed. Large figures of merit of the studied composites can promote hydroacoustic and piezoelectric energy-harvesting applications of the studied 2–1–2 composites.

Keywords: Composite · Piezoelectric Properties · PZN–xPT · Hydrostatic Figure of Merit · Energy-harvesting · Aspect Ratio

1 Introduction

A development in the field of piezo-active composites is associated with novel composite structures and components [1–4] which promote large hydrostatic, energy-harvesting, and other parameters for various applications that are based on an energy conversion. As is known, laminar composites with 2–2 connectivity (the notation in terms of work [5]) are characterised by a relatively simple composite structure and possibilities to modify it [4, 6–9] owing to an incorporation of a new component, pores, and so on. The modification of the laminar composite structure can lead to improved effective electromechanical (that is elastic, piezoelectric and dielectric) properties and related parameters [4, 6–10] of the 2–2-type composites and therefore can influence their effective electromechanical coupling factors, figures of merit, anisotropy factors, hydrostatic parameters etc.

I. A. Parinov et al. (Eds.): PHENMA 2023, SPM 41, pp. 151–166, 2024.
https://doi.org/10.1007/978-3-031-52239-0_15

Numerous results of studies show that the piezo-active 2–2-type composites based on relaxor-ferroelectric single crystals (SCs) [6, 10–12] with specific domain-engineered structures are of value and research interest due to their SC components that exhibit the outstanding electromechanical properties [13–17] including large piezoelectric coefficients d_{3j} and electromechanical coupling factors k_{3j}. Widespread domain-engineered relaxor-ferroelectric $(1 - x)Pb(Zn_{1/3}Nb_{2/3})O_3 - xPbTiO_3$ (PZN–xPT) and $(1 - y)Pb(Mg_{1/3}Nb_{2/3})O_3 - yPbTiO_3$ (PMN–yPT) SCs with the perovskite-type structure and compositions near the morphotropic phase boundary are suitable as components of the piezo-active 2–2-type composites [4, 6, 10–12, 18]. These SC components are often poled [13–17] along one of the following perovskite unit-cell directions: [0 0 1], [0 1 1] or [1 1 1], and for such SC components, full set of electromechanical constants were found during measurements (see, for instance, Refs. [13–17]).

A novel three-component SC/SC/polymer composite with 2–1–2 connectivity was put forward very recently [8], and the main component of this composite was domain-engineered lead-free SC poled along [0 0 1] of the perovskite unit cell. To the best knowledge, a systematic study on the 2–1–2 composites based on [0 1 1]-poled SCs was not yet carried out in detail, and only a few examples of the effective properties and related parameters of the 2–1–2 composites based on [0 1 1]-poled relaxor-ferroelectric SCs were discussed recently [9]. The aim of the present chapter is to analyse the piezoelectric properties and related figures of merit of the 2–1–2 composites wherein the main component is [0 1 1]-poled PZN–xPT SC, and the molar concentration x is related to compositions near the morphotropic phase boundary [13, 17–19].

2 Structure of the Composite, Its Effective Properties, Figures of Merit, and Components

The 2–1–2 composite shown in Fig. 1 is regarded as a system of the parallel-connected layers of two types [9], and the layers are arranged periodically along the OX_1 axis of the rectangular coordinate system $(X_1X_2X_3)$. The composite interfaces $x_1 = \text{const}$ are continuous along the OX_2 and OX_3 axes. The layer of the first type (LFT) in the composite represents relaxor-ferroelectric domain-engineered SC with the spontaneous polarisation vector $\vec{P}_s^{(1)} || OX_3$ and main crystallographic axes X, Y and Z (inset 1 in Fig. 1). This SC component is poled along [0 1 1] of the cubic (perovskite) unit cell. We use the notation 'SC-1' for this SC component that forms each LFT.

The layer of the second type (LST) represents a system of the aligned SC rods (SC-2 in our notation to be used in the text of the present chapter), and these rods are continuous along the OX_3 axis and periodically arranged in a polymer matrix (inset 2 in Fig. 1). The LST is characterised as a SC/polymer composite with 1–3 connectivity in terms of work [5]. The rod in the LST is in the form of an elliptic cylinder that is described by the equation $(x_1/a_1)^2 + (x_2/a_2)^2 = 1$ in the coordinate system $(X_1X_2X_3)$ (inset 3 in Fig. 1), where a_1 and a_2 are semiaxes of the ellipse. The aspect ratio of each rod base is given by $\eta_c = a_1/a_2$. The poling axis of the composite sample (see Fig. 1) is OX_3, and electrodes on this sample are perpendicular to the OX_3 axis.

The effective electromechanical properties of the 2–1–2 composite shown in Fig. 1 are found in two stages in accordance with the algorithm and formulae [8, 9]. The first

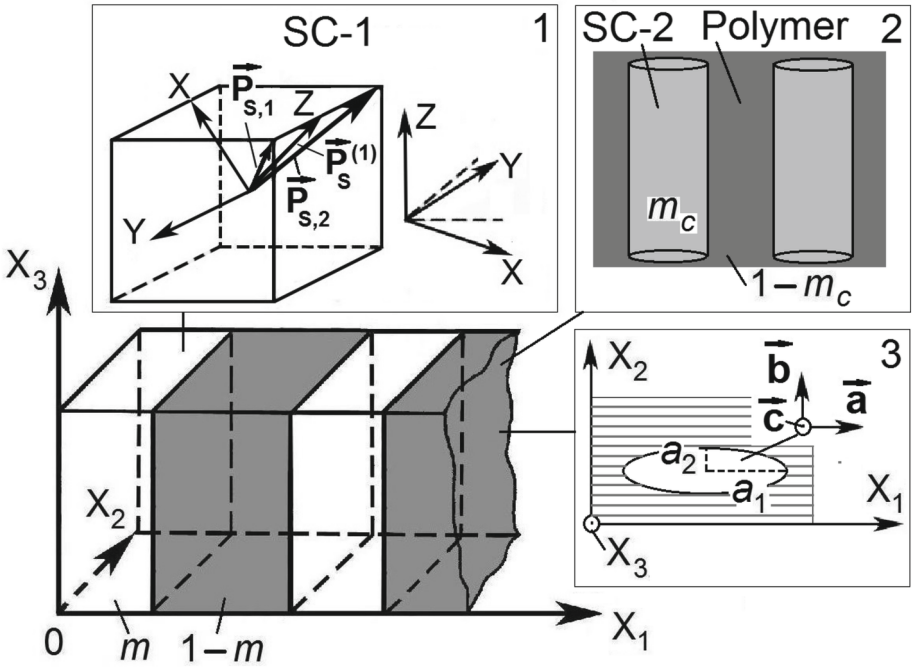

Fig. 1. Schematic of a 2–1–2 composite. m and $1-m$ are volume fractions of the LFTs and LSTs, respectively (reprinted from Topolov [9], with permission from Taylor and Francis). In inset 1, orientations of domains and main crystallographic axes X, Y and Z in SC-1 (LFT) are shown. In inset 2, the SC-2/polymer LST is shown. m_c and $1-m_c$ are volume fractions of SC-2 and polymer, respectively, in the LST. In inset 3, the elliptic cross section of the SC-2 rod and its unit-cell vectors a, b and c are shown. a_1 and a_2 are semiaxes of the ellipse (or the SC-2 rod base).

stage is associated with the application of the effective field method [6, 20] to evaluate the effective properties of the LST, that is the 1–3 SC/polymer composite with the regular distribution of the rods (see inset 2 in Fig. 1). In the second stage, the matrix method [6, 21] is used to evaluate the effective electromechanical properties of the 2–1–2 composite shown in Fig. 1. Both the effective field method and matrix method taken an electromechanical interaction into account. This interaction takes places between the structural elements of the composite (including the LST as an independent composite) due to the presence of the piezoelectric components. On the output, the matrix of the effective properties of the 2–1–2 composite has the form:

$$\|C^*\| = \begin{pmatrix} \|s^{*E}\| & \|d^*\|^t \\ \|d^*\| & \|\varepsilon^{*\sigma}\| \end{pmatrix},$$

where superscript 't' denotes the matrix transposition. The full set of the effective electromechanical properties in the $\|C^*\|$ matrix contains elastic compliances s_{ab}^{*E} at electric field $E = \text{const}$, piezoelectric coefficients d_{ij}^* and dielectric permittivities $\varepsilon_{fh}^{*\sigma}$ at mechanical stress $\sigma = \text{const}$. These effective properties, written in the general form as $\Pi^*(m,$

m_c, η_c), are found in the longwave approximation [4, 6, 10, 18]. Such an approximation holds on condition that a wavelength of an external acoustic field is much more than a width of each layer of the composite sample shown in Fig. 1.

Taking the effective electromechanical properties $\Pi^*(m,\ m_c,\ \eta_c)$ of the 2–1–2 composite into account, we analyse its hydrostatic piezoelectric coefficients:

$$d_h^* = d_{31}^* + d_{32}^* + d_{33}^* \ \text{ and } \ g_h^* = g_{31}^* + g_{32}^* + g_{33}^*, \tag{1}$$

hydrostatic figure of merit:

$$\left(Q_h^*\right)^2 = d_h^* g_h^*, \tag{2}$$

and energy-harvesting figures of merit:

$$\left(Q_{3j}^*\right)^2 = d_{3j}^* g_{3j}^* \tag{3}$$

that are associated with either the longitudinal piezoelectric effect (at $j = 3$) or transverse piezoelectric effect (at $j = 1$ and 2). The piezoelectric coefficients d_h^* and g_h^* from Eqs. (1) are used to characterise the hydrostatic activity and sensitivity [4, 6], respectively. The hydrostatic figure of merit $\left(Q_h^*\right)^2$ from Eq. (2) is of importance at estimations of a signal/noise ratio of a hydrophone [4, 6, 10, 22] at hydrostatic loading. The energy-harvesting figures of merit $\left(Q_{3j}^*\right)^2$ from Eq. (3) are used [4, 6, 7, 10, 18] to estimate the signal/noise ratio of a transducer by taking the piezoelectric effect (longitudinal or transverse) into consideration. The figures of merit $\left(Q_h^*\right)^2$ and $\left(Q_{3j}^*\right)^2$ from Eqs. (2) and (3) are also used to describe a mechanical-to-electric energy conversion in piezoelectric materials and to show their effectiveness in the context of the energy conversion and energy harvesting [4, 6, 7, 10].

The main piezoelectric component of the 2–1–2 composites studied by us is domain-engineered PZN–xPT SC poled along [0 1 1] of the perovskite unit cell. Domain orientations in such a poled state are shown in inset 1 of Fig. 1. Full sets of electromechanical constants of PZN–xPT SCs at $0.0475 \le x \le 0.09$ [16, 17, 26] are shown in Table 1, and these PZN–xPT compositions are located close to the morphotropic phase boundary [19]. It should be added that domain-engineered PZN–xPT SCs poled along [0 1 1] were considered [18] as main components of the advanced 2–2-type composites wherein an appreciable orientation effect was described. The second piezoelectric component of each 2–1–2 composite from our present study is $Li_2B_4O_7$ (LBO) SC [23] that exhibits a unique anisotropy of the piezoelectric and elastic properties (see the full set of electromechanical constants in Table 2). The SC components from the LFT and LST differ by symmetry, see data in Tables 1 and 2. The LST of the composite contains polyethylene (PE) that is regarded as a piezo-passive isotropic component [4, 24] with constants listed in Table 2.

Table 1. Room-temperature elastic compliances s^E_{ab}, piezoelectric coefficients d_{ij} and dielectric permittivities ε^σ_{pp} of domain-engineered [0 1 1]-poled PZN–xPT SCs with macroscopic $mm2$ symmetry

Constants	$x = 0.0475$, Ref. [17]	$x = 0.055$, Ref. [17]	$x = 0.065$, Ref. [17]	$x = 0.07$, Ref. [16]	$x = 0.09$, Ref. [26]
s^E_{11}, 10^{-12} Pa^{-1}	34.26	39.04	46.99	67.52	73.07
s^E_{12}, 10^{-12} Pa^{-1}	−47.45	−56.67	−74.01	−60.16	−63.98
s^E_{13}, 10^{-12} Pa^{-1}	26.05	32.65	39.51	3.355	4.256
s^E_{22}, 10^{-12} Pa^{-1}	125.35	137.40	170.69	102.0	125.6
s^E_{23}, 10^{-12} Pa^{-1}	−74.22	−85.47	−96.76	−54.47	−68.04
s^E_{33}, 10^{-12} Pa^{-1}	51.32	60.68	61.47	62.02	67.49
s^E_{44}, 10^{-12} Pa^{-1}	14.68	15.46	15.04	15.45	15.12
s^E_{55}, 10^{-12} Pa^{-1}	277.78	294.12	333.33	291.5	299.3
s^E_{66}, 10^{-12} Pa^{-1}	125.98	155.29	169.08	14.08	16.54
d_{15}, pC/N	4037	4187	4871	1823	2012
d_{24}, pC/N	134	207	121	50	118.7
d_{31}, pC/N	750	858	1191	478	476.0
d_{32}, pC/N	−1852	−1985	−2618	−1460	−1705
d_{33}, pC/N	1185	1319	1571	1150	1237
$\varepsilon^\sigma_{11}/\varepsilon_0$	8000	8500	9500	8240	8740
$\varepsilon^\sigma_{22}/\varepsilon_0$	2600	3050	1500	1865	2075
$\varepsilon^\sigma_{33}/\varepsilon_0$	3900	4000	5600	3180	3202

Table 2. Room-temperature elastic moduli c_{ab}^{E}, piezoelectric coefficients e_{ij} and dielectric permittivity ε_{pp}^{ξ} of LBO SC (4 mm symmetry) and PE (isotropic medium)

Constants	LBO SC, Ref. [23]	PE, Refs. [4, 24]
c_{11}^{E}, 10^{10} Pa	13.5	0.0778
c_{12}^{E}, 10^{10} Pa	0.357	0.0195
c_{13}^{E}, 10^{10} Pa	3.35	0.0195
c_{33}^{E}, 10^{10} Pa	5.68	0.0778
c_{44}^{E}, 10^{10} Pa	5.85	0.0292
c_{66}^{E}, 10^{10} Pa	4.67	0.0292
e_{15}, C/m^2	0.472	0
e_{31}, C/m^2	0.290	0
e_{33}, C/m^2	0.928	0
$\varepsilon_{11}^{\xi}/\varepsilon_0$	8.90	2.3
$\varepsilon_{33}^{\xi}/\varepsilon_0$	8.07	2.3

Taking the microgeometry of the composite (Fig. 1) and symmetry of the aforementioned components into account, we represent the matrix of the piezoelectric coefficients d_{ij}^{*} as

$$||d^{*}| = \begin{bmatrix} 0 & 0 & 0 & 0 & d_{15}^{*} & 0 \\ 0 & 0 & 0 & d_{24}^{*} & 0 & 0 \\ d_{31}^{*} & d_{32}^{*} & d_{33}^{*} & 0 & 0 & 0 \end{bmatrix}.$$

The matrix of the piezoelectric voltage coefficients $\|g^{*}\|$ of the composite has the similar form, and elements of the $\|g^{*}\|$ matrix can be evaluated by using the formula [25]

$$d_{fk}^{*} = \varepsilon_{fj}^{*\sigma} g_{jk}^{*}. \tag{4}$$

In Eq. (4), the dielectric permittivity $\varepsilon_{fj}^{*\sigma}$ and piezoelectric coefficient d_{fk}^{*} are taken as elements of the $\|C^{*}\|$ matrix. Considering Eqs. (2) and (4) as well as the symmetry of the components of the composite, one can write its hydrostatic figure of merit as

$$\left(Q_h^{*}\right)^2 = \left(d_h^{*}\right)^2 / \varepsilon_{33}^{*\sigma}. \tag{5}$$

Comparing the piezoelectric performance of [0 1 1]-poled PZN–xPT SCs from Table 1, we note the large piezoelectric coefficients d_{15} and $|d_{32}|$. Our analysis of the effective piezoelectric properties of the 2–1–2 composite suggests that the piezoelectric coefficient $d_{32}^{(1)}$ of PZN–xPT SC in the LFT influences the effective piezoelectric coefficient d_{32}^{*} of the composite to a large extent. This is accounted for by the continuous

distribution of SC-1 as a piezoelectric component along the OX_2 and OX_3 axes, see Fig. 1. Therefore, the piezoelectric coefficient d_{32}^* can lead to a large negative contribution in the hydrostatic piezoelectric coefficient d_h^* from Eqs. (1), and this will promote decreasing d_h^* of the composite. To avoid this decreasing d_h^* and its influence on the hydrostatic figure of merit $\left(Q_h^*\right)^2$ from Eq. (2), we consider the rotation of the main crystallographic axes X and Y of PZN–xPT SC around the Z axis (see inset 1 in Fig. 1) by 90° clockwise [9]. Such an orientation of the X and Y axes in each LFT leads to an influence of the negative $d_{32}^{(1)}$ of PZN–xPT SC on the lateral piezoelectric effect in the composite along the OX_1 axis, and then the positive $d_{31}^{(1)}$ of PZN–xPT SC will influence the lateral piezoelectric effect in the composite along the OX_2 axis (Fig. 1). Along the OX_2 axis shown in Fig. 1, the continuous distribution of the LFT with the high piezoelectric activity is observed. Moreover, a decrease of $\left|d_{31}^*\right|$ is achieved due to the interfaces $x_1 = \text{const}$ and due to the heavily oblate shape of each rod base in the LST, i.e., on condition $\eta_c \gg 1$ (see inset 3 in Fig. 1). Such a shape of the rod base promotes a small elastic compliance $s_{11}^{(2),E}$ of the LST in comparison to its $s_{22}^{(2),E}$, and the large $s_{22}^{(2),E}$ is important to achieve the large piezoelectric coefficient d_{32}^* of the composite and the related large positive contribution in the hydrostatic piezoelectric coefficient d_h^*.

Considering the pointed orientation of the main crystallographic X and Y axes of SC-1 in the LFT (see inset 1 in Fig. 1), we represent the electromechanical properties $\Pi^{(1)}$ of each LFT in the $(X_1X_2X_3)$ system as follows:

$$\begin{gathered} s_{11}^{(1),E} = s_{22}^E, s_{12}^{(1),E} = s_{12}^E, s_{13}^{(1),E} = s_{23}^E, s_{22}^{(1),E} = s_{11}^E, s_{23}^{(1),E} = s_{12}^E, \\ s_{33}^{(1),E} = s_{33}^E, s_{44}^{(1),E} = s_{55}^E, s_{55}^{(1),E} = s_{44}^E, s_{66}^{(1),E} = s_{66}^E, d_{31}^{(1)} = d_{32}, \\ d_{32}^{(1)} = d_{31}, d_{33}^{(1)} = d_{33}, d_{15}^{(1)} = d_{24}, d_{24}^{(1)} = d_{15}, \varepsilon_{11}^{(1),\sigma} = \varepsilon_{22}^\sigma, \varepsilon_{22}^{(1),\sigma} = \varepsilon_{11}^\sigma, \\ \text{and } \varepsilon_{33}^{(1)\sigma} = \varepsilon_{33}^\sigma. \end{gathered} \tag{6}$$

In Sect. 3, we show and discuss new results on the effective parameters (1)–(3) of the 2–1–2 composites based on [0 1 1]-poled PZN–xPT SCs.

3 Results and Discussion

3.1 Hydrostatic Figures of Merit $\left(Q_h^*\right)^2$ of Composites Based on PZN–xPT

Figure 2 shows that the largest hydrostatic figure of merit $\left(Q_h^*\right)^2$ from Eq. (2) is achieved in the 2–1–2 composite at $x = 0.065$. This is due to the larger piezoelectric coefficients $\left|d_{32}^{(1)}\right|$ and $d_{33}^{(1)}$ of PZN–0.065PT SC (see Table 1) as a main component of the composite. This component promotes the large piezoelectric coefficients $d_{33}^* > 0$ and $d_{32}^* > 0$ which give a decisive contribution [9] in the hydrostatic piezoelectric coefficient d_h^* from Eqs. (1) and in the hydrostatic figure of merit $\left(Q_h^*\right)^2$ from Eqs. (2) and (5).

The diagram in Fig. 2 was built at the relatively small volume fractions of PZN–xPT SC, namely, $m = 0.1$ and 0.2. At these and smaller m values, the dielectric permittivity $\varepsilon_{33}^{*\sigma}$ of the composite is small in comparison to $\varepsilon_{33}^{(1),\sigma}$ of PZN–xPT SC, and therefore, cannot lead to a significant decrease of the hydrostatic figure of merit $\left(Q_h^*\right)^2 \sim 1/\varepsilon_{33}^{*\sigma}$ in accordance with Eq. (5).

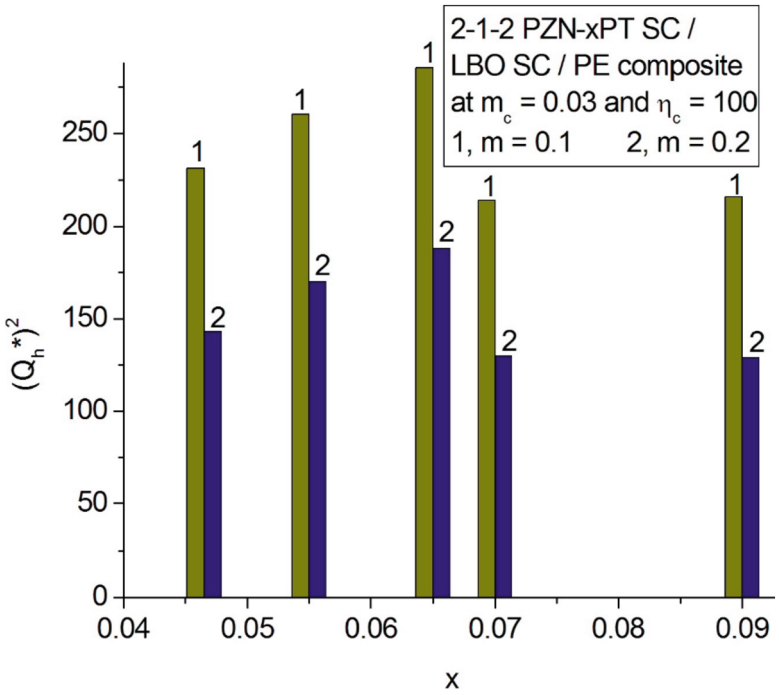

Fig. 2. Molar-concentration (x) dependences of the hydrostatic figure of merit $\left(Q_h^*\right)^2$ (in 10^{-12} Pa^{-1}) of 2–1–2 PZN–xPT SC/LBO SC/PE composites at $m = \text{const}$ (reprinted from Topolov [9], with permission from Taylor and Francis).

3.2 Volume-Fraction (m) Dependence of Hydrostatic Parameters

Graphs in Fig. 3 show the non-monotonic volume-fraction (m) behavior of the hydrostatic parameters (1) and (2). The dielectric permittivity $\varepsilon_{33}^{*\sigma}$ of the composite is an increasing function as is known from studies on the parallel-connected 2–2-type composites [4, 6, 9], and at small volume fractions of SC-1 (that is at $m \ll 1$), $\varepsilon_{33}^{*\sigma} \ll \varepsilon_{33}^{(1),\sigma}$. The small $\varepsilon_{33}^{*\sigma}$ values promote large values of g_h^* from Eqs. (1) and sharp max g_h^*, see curve 2 in Fig. 3. In comparison to this feature, max d_h^* is less pronounced and observed at relatively large volume fractions m of PZN–xPT SC, see curve 1 in Fig. 3.

Maxima of $\left(Q_h^*\right)^2$ from Eq. (2) are located in an intermediate region of volume fractions m, see curve 3 in Fig. 3. This is associated with the influence of the dielectric permittivity $\varepsilon_{33}^{*\sigma}$ on $\left(Q_h^*\right)^2$ in accordance with Eq. (5) and the inequality $\varepsilon_{33}^{*\sigma} \ll \varepsilon_{33}^{(1),\sigma}$ that holds at $m \ll 1$. The less sharp character of max $[\left(Q_h^*\right)^2]$ in comparison to max g_h^* (see curves 2 and 3 in Fig. 3) can be accounted for by the relationship $\left(Q_h^*\right)^2 \sim \left(d_h^*\right)^2$ that follows from Eq. (5).

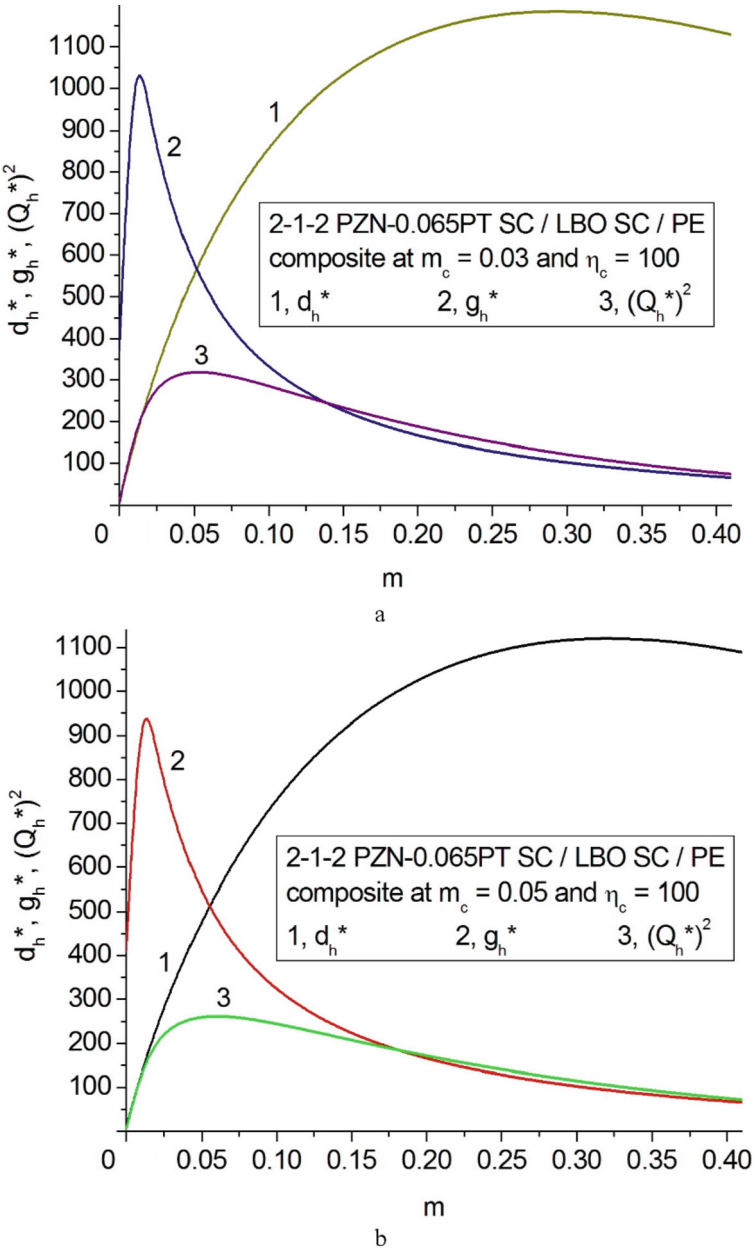

Fig. 3. Volume-fraction (m) dependences of the hydrostatic piezoelectric coefficient d_h^* (in pC/N), piezoelectric coefficient g_h^* (in mV·m/N) and figure of merit $\left(Q_h^*\right)^2$ (in 10^{-12} Pa^{-1}) of the 2–1–2 PZN–0.065PT SC/LBO SC/PE composite ar $m_c = 0.03$ (graph a) or $m_c = 0.05$ (graph b) in the LST.

3.3 Links Between Piezoelectric Properties and Figures of Merit

Relationships between the piezoelectric properties and energy-harvesting figures of merit $\left(Q_{3j}^*\right)^2$ are illustrated by Fig. 4. Maxima of g_{3j}^* (see curves 5 and 6 in Fig. 4, a) and $\left(Q_{3j}^*\right)^2$ (see curves 2 and 3 in Fig. 4, b) obey the following similar inequalities:

$$\max g_{33}^* > \max g_{32}^* \text{ and } \max\left[\left(Q_{33}^*\right)^2\right] > \max\left[\left(Q_{32}^*\right)^2\right]. \tag{7}$$

However, the figure of merit $\left(Q_{31}^*\right)^2$ increases monotonously (see curve 1 in Fig. 4, b) at the non-monotonic dependence of g_{31}^* (see curve 4 in Fig. 4, b) and cannot be involved in formulae (7) or similar relations. The reason of such an inconsistent volume-fraction behavior is concerned with the relatively small $\left|\min g_{31}^*\right|$ value and monotonic increase of d_{31}^* (see curves 1 and 4 in Fig. 4, a). The presence of the interfaces $x_1 = \text{const}$ in the composite (see Fig. 1) strongly influences the piezoelectric effect associated with both d_{31}^* and g_{31}^*. Therefore, the volume-fraction dependence of $\left(Q_{31}^*\right)^2$ evaluated in accordance with Eq. (3) differs from the volume-fraction $\left(Q_{33}^*\right)^2$ and $\left(Q_{32}^*\right)^2$ dependences, see Fig. 4, b. It should be added that the inequality:

$$\max\left[\left(Q_{33}^*\right)^2\right] < \max\left[\left(Q_h^*\right)^2\right] \tag{8}$$

holds, see curve 3 in Fig. 3, a and curve 3 in Fig. 4, b. Condition (8) is in contradiction with the inequality $\max\left[\left(Q_{33}^*\right)^2\right] > \max\left[\left(Q_h^*\right)^2\right]$ that is valid [4, 6, 27, 28] in many 2–2-type composites based on perovskite ferroelectric ceramics or domain engineered SCs poled along [0 0 1].

The validity of condition (8) is accounted for specifics of the piezoelectric effect in the [0 1 1]-poled SC component, for example PZN–0.065PT in the present case. As seen in Table 1, the piezoelectric coefficients d_{3j} of [0 1 1]-poled PZN–0.065PT SC obey the inequality $d_{31} < d_{33} < |d_{32}|$ that differs from conditions $d_{31} = d_{32}$ and $|d_{32}| < d_{33}$ which hold in [0 0 1]-poled PZN–xPT, PMN–yPT [6, 10, 14] and other SCs.

3.4 Maxima of Figures of Merit at Variations of the Aspect Ratio η_c

Our results, shown in Figs. 2, 3 and 4, are obtained for the 2–1–2 composite with the SC rods at the aspect ratio of their bases $\eta_c = 100$. Changes of the aspect ratio η_c led to changes of the elastic properties of the LST, and this influences the piezoelectric response of the composite along the OX_1 and OX_2 axes. We remind the reader that each SC rod is oriented as shown in inset 3 of Fig. 1, and such an orientation is inseparably linked with orientations of the OX_1 and OX_2 axes.

Table 3 contains data on local maxima of figures of merit $\left(Q_{3j}^*\right)^2$ and $\left(Q_h^*\right)^2$ which are evaluated for the composite at various aspect ratios η_c from 50 (at $a_1 \gg a_2$, as shown in inset 3 of Fig. 1) to 0.01 (at $a_1 \ll a_2$,). The volume fraction of the SC rods in the LST is $m_c = 0.03$, that is the polymer component occupies a large area on the (X_1OX_2) plane (see Fig. 1). The figure of merit $\left(Q_{33}^*\right)^2$ concerned with the longitudinal

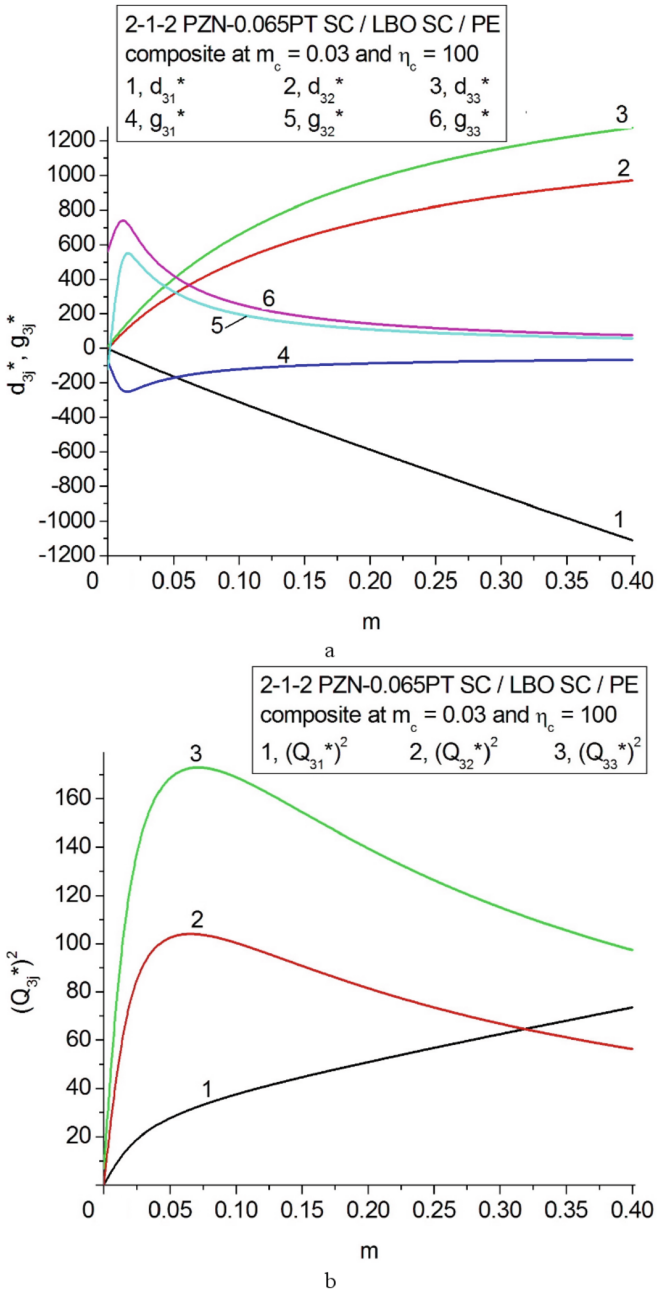

Fig. 4. Volume-fraction (m) dependences of piezoelectric coefficients d_{3j}^* (a, in pC/N) and g_{3j}^* (a, in mV·m/N) and figures of merit $\left(Q_{3j}^*\right)^2$ (b, in 10^{-12} Pa^{-1}) of the 2–1–2 PZN–0.065PT SC/LBO SC/PE composite.

piezoelectric effect does not undergo changes of local max$[(Q^*_{33})^2]$ because the rod base changes the semiaxes a_1 and/or a_2 in the perpendicular direction (see insets 2 and 3 in Fig. 1). The figure of merit $(Q^*_{31})^2$ is characterised by the monotonic dependence (see, for example curve 1 in Fig. 4, b). A decrease of the aspect ratio η_c from 50 to 1 does not lead to appreciable changes of values of local max$[(Q^*_{32})^2]$, see the 2nd column of Table 3. Within the same η_c range, local max$[(Q^*_h)^2]$ undergoes changes, however its value decreases by ca. 10%, as shown in the 3rd column of Table 3. It is important to underline that the aforementioned local maxima at $\eta_c \geq 1$ are observed at the almost equal volume fractions $m \approx 0.05$–0.06.A further decrease of η_c from 1 to 0.01 causes noticeable changes of local maxima of both $(Q^*_{32})^2$ and $(Q^*_h)^2$ (see Table 3) as well as displacements of locations of these maxima. The aspect ratio $\eta_c \ll 1$ corresponds to an elliptic cylinder with the base semiaxes that obey the inequality $a_1 \ll a_2$.

Table 3. Local maxima of figures of merit $(Q^*_{3j})^2$ and $(Q^*_h)^2$ (in 10^{-12} Pa^{-1}) of the 2–1–2 0.065PT SC/LBO SC/PE composite at $mc = 0.03$ and variations of the aspect ratio η_c

η_c	max$[(Q^*_{32})^2]$	max$[(Q^*_h)^2]$
50	105 (at $m = 0.064$)	306 (at $m = 0.060$)
20	105 (at $m = 0.063$)	292 (at $m = 0.058$)
10	106 (at $m = 0.063$)	283 (at $m = 0.052$)
5	106 (at $m = 0.063$)	278 (at $m = 0.052$)
2	105 (at $m = 0.063$)	274 (at $m = 0.052$)
1	105 (at $m = 0.064$)	272 (at $m = 0.052$)
0.5	104 (at $m = 0.065$)	269 (at $m = 0.053$)
0.1	96.9 (at $m = 0.073$)	255 (at $m = 0.055$)
0.05	89.9 (at $m = 0.083$)	241 (at $m = 0.059$)
0.01	64.2 (at $m = 0.140$)	182 (at $m = 0.073$)

Note. Local max$[(Q^*_{33})^2] = 174 \times 10^{-12}$ Pa^{-1} is achieved at the volume fraction $m = 0.070$ irrespective of the aspect ratio η_c in the LST.

Variations of the aspect ratio η_c lead to changes of the elastic compliances $s^{(2),E}_{ab}$ in the LST. In Fig. 5, the aspect-ratio dependence of $s^{(2),E}_{ab}$ is graphically represented for $ab = 11$, 12, …, and 33. The shear elastic compliances $s^{(2),E}_{44}$, $s^{(2),E}_{55}$ and $s^{(2),E}_{66}$ do not influence the piezoelectric response associated with the piezoelectric coefficients d^*_{3j} or g^*_{3j} of the composite, where $j = 1$, 2 and 3. The behavior of $s^{(2),E}_{ab}$ shows that only $s^{(2),E}_{11}$ and $s^{(2),E}_{12}$ (see curves 1 and 2 in Fig. 5) undergo noticeable changes on decreasing η_c, and stimulates changes of the piezoelectric coefficients d^*_{3j} and g^*_{3j} ($j = 1$ and 2) and figures of merit $(Q^*_{31})^2$, $(Q^*_{32})^2$ and $(Q^*_h)^2$ of the composite. At $\eta_c < 1$, a decrease of

$\left(Q_{32}^*\right)^2$ and $\left(Q_h^*\right)^2$ is caused by a lower piezoelectric activity of the composite along the OX_2 axis. In this case, a contribution from the piezoelectric coefficient d_{32}^* to d_h^*, $\left(Q_h^*\right)^2$ and $\left(Q_{32}^*\right)^2$ [see Eqs. (1)–(3)] becomes smaller due to increasing the elastic compliances $s_{11}^{(2),E}$ and $\left|s_{12}^{(2),E}\right|$ (see Fig. 5) in the LST.

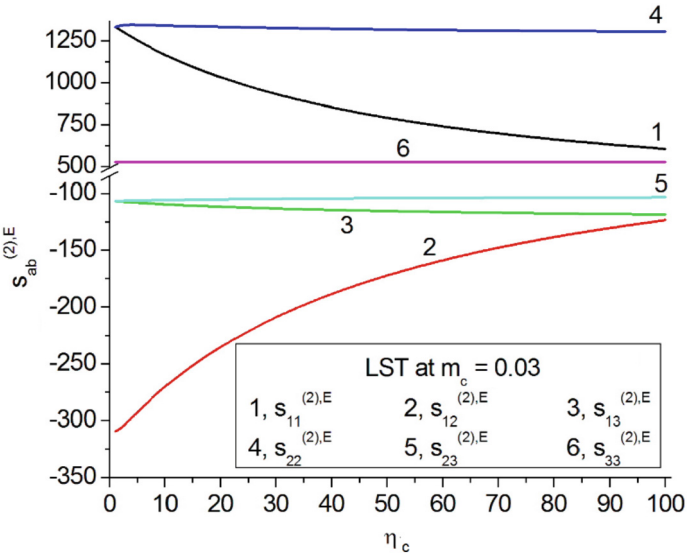

Fig. 5. Elastic compliances $s_{ab}^{(2),E}$ (in 10^{-12} Pa^{-1}) of the LBO SC/PE LST at $m_c = 0.03$ (reprinted from Topolov [9], with permission from Taylor and Francis).

3.5 Comparison to Data on Some 2–2-Type Composites

The studied 2–1–2 composites based on [0 1 1]-poled PZN–xPT SCs are characterised by large hydrostatic figures of merit $\left(Q_h^*\right)^2$ (Fig. 2), and the $\left(Q_h^*\right)^2$ values at the relatively small volume fraction $m = 0.1$ or 0.2 are by approximately an order-of-magnitude larger than $\left(Q_h^*\right)^2$ of conventional 2–2 ferroelectric ceramic/polymer composites [4, 6, 29]. The $\left(Q_h^*\right)^2$ values at $m = 0.1$ or 0.2 (see Fig. 2) are larger than $\left(Q_h^*\right)^2$ of 2–2 composites based on [0 1 1]-poled PMN–yPT SCs [11]. The 2–1–2 composite based on [0 1 1]-poled PZN–0.065PT SC with the set of electromechanical constants from Eqs. (6) is of value due to the large hydrostatic parameters d_h^*, g_h^* and $\left(Q_h^*\right)^2$, and energy-harvesting figure of merit $\left(Q_{33}^*\right)^2$ (see Figs. 3 and 4, and Table 3). These parameters indicate advantages of the 2–1–2 composite over 2–0–2–0 composites [27, 28] that contain the porous ferroelectric PZT-type ceramic and porous polymer layers. The $\left(Q_h^*\right)^2$ values of the 2–1–2 composite based on [0 1 1]-poled PZN–0.065PT SC are larger than $\left(Q_h^*\right)^2$ of a 2–1–2 lead-free composite [8] wherein the main SC component is replaced by [0 0 1]-poled domain engineered SC from solid solutions of alkali niobates-tantalates [30]. Despite a high

piezoelectric sensitivity of lead-free [0 0 1]-poled domain-engineered SC [30], this SC component from work promotes the smaller d_h^* and $\left(Q_h^*\right)^2$ values of the 2–1–2 composite from work [8].

4 Conclusion

In the present chapter, results on the novel high-performance 2–1–2 composites based on [0 1 1]-poled PZN–xPT SCs have been shown, and specifics of the hydrostatic piezoelectric response and figures of merit of these composites have been discussed. Molar concentrations x have been chosen near the morphotropic ohase boundary to provide a high piezoelectric activity of PZN–xPT SCs (Table 1). The due orientation of the main crystallographic axes of this SC component in the LFT (inset 1 in Fig. 1) and the related set of its electromechanical constants from Eqs. (6) lead to the large hydrostatic piezoelectric coefficients d_h^*, g_h^* and figure of merit $\left(Q_h^*\right)^2$ from Eqs. (1) and (2). In the LST, changes of the aspect ratio η_c of the SC rod base (insets 2 and 3 in Fig. 1) influence d_h^*, g_h^*, $\left(Q_h^*\right)^2$, and energy-harvesting figures of merit $\left(Q_{31}^*\right)^2$ and $\left(Q_{32}^*\right)^2$ of the composite.

Large values of the hydrostatic figure of merit $\left(Q_h^*\right)^2 > 2 \cdot 10^{-10}$ Pa^{-1} and energy-harvesting figures of merit $\left(Q_{33}^*\right)^2 \sim 10^{-10}$ Pa^{-1} and $\left(Q_{32}^*\right)^2 \sim 10^{-10}$ Pa^{-1} are achieved in the 2–1–2 composite based on [0 1 1]-poled PZN–0.065PT SC (Figs. 2, 3 and 4) at relatively small volume fractions m_c of the LBO SC rods in the LST. The effect of the aspect ratio η_c of the rod base and the influence of the elastic properties of the LST on the piezoelectric performance and figures of merit if the composite has been analysed at small volume fractions m_c of SC-2 in the LST. The best sets of the effective parameters (1)–(3) of the composite are achieved at aspect ratios $\eta_c \gg 1$ and volume fractions of LBO SC $m_c \ll 1$ in the LST. Due to the large figures of merit $\left(Q_h^*\right)^2$, $\left(Q_{33}^*\right)^2$ and $\left(Q_{32}^*\right)^2$, the studied 2–1–2 composites can be of value as active elements in modern hydroacoustic and piezoelectric energy-harvesting devices or systems.

Acknowledgements. The author would like to thank Prof. Dr. A. E. Panich and Prof. Dr. I. A. Parinov (Southern Federal University, Russia), Prof. Dr C. R. Bowen (University of Bath, UK), and Prof. Dr. P. Bisegna (University of Rome Tor Vergata, Italy) for their interest in the field of modern piezo-active composites. This research was supported by the Southern Federal University (research topic "Development and Materials-Science Substantiation of the Creation of Materials and Products Based on Piezoelectric Ceramics Using Additive Technologies", contract No. 176/22-D, July 11th, 2022).

References

1. Wu, J., Ma, W., Chi, M., Wang, S., Zhang, P.: Effect of surface modification of ferroelectric ceramic component on the properties of PZT-type/epoxy piezoelectric composite with spiral structure. J. Alloys Compd. **820**, 153362 (2020)
2. Hoffmann, P., Köllner, D., Simon, S., Kakimoto, K.-I., Fey, T.: Modular lead-free piezoceramic/polymer composites with locally adjustable piezoelectric properties. Open Ceram. **13**, 100320 (2023)

3. Khanbareh, H., Topolov, V.Yu., Bowen, C.R.: Piezo-Particulate Composites. Manufacturing, Properties Applications. Springer, Cham (2019). https://doi.org/10.1007/978-3-030-19204-4
4. Roscow, J.I., Topolov, V.Yu., Bowen, C.R., Khanbareh, H.: Innovative Piezo-Active Composites and Their Structure – Property Relationships. World Scientific, Singapore (2022). https://doi.org/10.1142/13003
5. Newnham, R.E., Skinner, D.P., Cross, L.E.: Connectivity and piezoelectric – pyroelectric composites. Mater. Res. Bull. **13**(5), 525–536 (1978)
6. Topolov, V.Yu., Bowen, C.R., Bisegna, P.: Piezo-Active Composites. Microgeometry – Sensitivity Relations. Springer, Cham (2018). https://doi.org/10.1007/978-3-319-93928-5
7. Isaeva, A.N., Topolov, V.Yu., Bowen, C.R., Roscow, J.I.: Twelve modified figures of merit of 2–2-type composites based on relaxor-ferroelectric single crystals. Mater. Chem. Phys. **279**, 125691 (2022)
8. Topolov, V.Yu.: Novel lead-free 2–1–2 composite: predicted high piezoelectric sensitivity and significant hydrostatic response. Smart Mater. Struct. **32**(8), 085010 (2023)
9. Topolov, V.Yu.: Novel piezo-active 2–1–2 composites with sets of large hydrostatic parameters. Ferroelectrics Lett. Sec. **50**(4–6), 102–117 (2023)
10. Bowen, C.R., Topolov, V.Yu., Kim, H.A.: Modern Piezoelectric Energy-Harvesting Materials. Springer, Cham (2016). https://doi.org/10.1007/978-3-319-29143-7
11. Li, L., Zhang, S., Xu, Z., Geng, X., Luo, J., Shrout, T.: Hydrostatic piezoelectric properties of [011] poled $Pb(Mg_{1/3}Nb_{2/3})O_3$-$PbTiO_3$ single crystals and 2–2 lamellar composites. Appl. Phys. Lett. **104**(3), 032909 (2014)
12. Yue, Q., et al.: Design and fabrication of relaxor-ferroelectric single crystal PIN–PMN–PT/epoxy 2–2 composite based array transducer. Sens. Actuators A Phys. **234**, 34–42 (2015)
13. Yin, J., Jiang, B., Cao, W.: Elastic, piezoelectric, and dielectric properties of $0.955Pb(Zn_{1/3}Nb_{2/3}O_3$-$O.45PbTi0_3$ single crystal with designed multidomains. IEEE Trans. Ultrason. Ferroelec. Freq. Control **47**(1), 285–291 (2000)
14. Zhang, R., Jiang, B., Cao, W.: Elastic, piezoelectric, and dielectric properties of multidomain $0.67Pb(Mg_{1/3}Nb_{2/3})O_3 - 0.33PbTiO_3$ single crystals. J. Appl. Phys. **90**(7), 3471–3475 (2001)
15. Liu, X., Zhang, S., Luo, J., Shrout, T., Cao, W.: Complete set of material constants of $Pb(In_{1/2}Nb_{1/2})O_3$–$Pb(Mg_{1/3}Nb_{2/3})O_3$–$PbTiO_3$ single crystal with morphotropic phase boundary composition. J. Appl. Phys. **106**(7), 074112 (2009)
16. He, C., Jing, W., Wang, F., Zhu, K., Qiu, J.: Full tensorial elastic, piezoelectric, and dielectric properties characterization of [011]-poled PZN-9%PT single crystal. IEEE Trans. Ultrason. Ferroelec. Freq. Control **58**(6), 1127–1130 (2011)
17. Zhang, S., Lim, L.C.: Property matrices of [011]-poled rhombohedral $Pb(Zn_{1/3}Nb_{2/3})O_3$-(4.5–7)%$PbTiO_3$ single crystals. AIP Adv. **8**(11), 115010 (2018)
18. Topolov, V.Yu., Bowen, C.R., Krivoruchko, A.V., Isaeva, A.N.: Orientation effects and figures of merit in advanced 2-2-type composites based on [011]-poled domain-engineered single crystals. CrystEngComm **24**(6), 1177–1188 (2022)
19. La-Orauttapong, D., Noheda, B., Ye, Z.-G., Gehring, P.M., Cox, D.E., Shirane, G.: Phase diagram of the relaxor ferroelectric $(1 - x)Pb(Zn_{1/3}Nb_{2/3})O_3 - xPbTiO_3$. Phys. Rev. B **65**(14), 144101 (2002)
20. Huang, J.H., Kuo, W.-S.: Micromechanics determination of the effective properties of piezoelectric composites containing spatially oriented short fibers. Acta Mater. **44**(12), 4889–4898 (1996)
21. Levassort, F., Lethiecq, M., Certon, D., Patat, F.: A matrix method for modeling electroacoustic moduli of 0–3 piezocomposites. IEEE Trans. Ultrason. Ferroelec. Freq. Control **44**(2), 445–452 (1997)
22. Sherman, C.H., Butler, J.L.: Transducers and Arrays for Underwater Sound. Springer, New York (2007). https://doi.org/10.1007/978-0-387-33139-3

23. Adachi, M., Shiosaki, T., Kobayashi, H., Ohnishi, O., Kawabata, A.: Temperature compensated piezoelectric lithium tetraborate crystal for high frequency surface acoustic wave and bulk wave device applications. In: Proceedings of the IEEE Ultrasonics Symposium, October 1985, pp. 228–232. IEEE, New York (1985)
24. Evans, K.E., Alderson, K.L.: The static and dynamic moduli of auxetic microporous polyethylene. J. Mater. Sci. Lett. **11**(22), 1721–1724 (1992). https://doi.org/10.1007/BF00736221
25. Ikeda, T.: Fundamentals of Piezoelectricity. Oxford University Press, Oxford/New York/Toronto (1990)
26. Zhang, R., Jiang, B., Jiang, W., Cao, W.: Complete set of elastic, dielectric, and piezoelectric coefficients of $0.93Pb(Zn_{1/3}Nb_{2/3})O_3$–$0.07PbTiO_3$ single crystal poled along [011]. Appl. Phys. Lett. **89**(24), 242908 (2006)
27. Nesterov, A.A., Topolov, V.Yu., Tolstunov, M.I., Isaeva, A.N.: Improved piezoelectric performance and hydrostatic parameters of a novel 2–0–2–0 composite. Mater. Lett. **252**(1), 150–152 (2019)
28. Nesterov, A.A., Topolov, V.Yu., Tolstunov, M.I., Isaeva, A.N.: Longitudinal piezoelectric effect and hydrostatic response in novel laminar composites based on ferroelectric ceramics. Ceram. Int. **45**(17), 22241–22248 (2019)
29. Akdogan, E.K., Allahverdi, M., Safari, A.: Piezoelectric composites for sensor and actuator applications. IEEE Trans. Ultrason. Ferroelec. Freq. Control **52**(5), 746–775 (2005)
30. Huo, X., et al.: (K, Na, Li)(Nb, Ta)O_3: Mn lead-free single crystal with high piezoelectric properties. J. Am. Ceram. Soc. **98**(6), 1829–1835 (2015)